Implementation of Particle Image Velocimetry for the Evaluation of the Bearing Capacity and the Failure Mechanism of Strip Footings on Reinforced Sand Slope

Nabeel K. Lwti
Al-Furat Al-Awsat Technical University, 31001, Al-Najaf, Iraq
nabeelkl@atu.edu.iq (corresponding author)

Balqees A. Ahmed
Department of Civil Engineering, University of Baghdad, Baghdad, Iraq
balqees.a@coeng.uobaghdad.edu.iq

Received: 10 June 2025 | Revised: 8 July 2025 and 23 July 2025 | Accepted: 29 July 2025

 DOI: https://doi.org/10.48084/etasr.12654

ABSTRACT

This study presents a series of small-scale physical model tests designed to investigate the bearing capacity and failure mechanisms of strip footings located on the crest of reinforced and unreinforced sand slopes using Particle Image Velocimetry (PIV) techniques. A total of 30 laboratory model tests were performed under varied conditions of setback distance, relative density, and reinforcement. A single geotextile-reinforced layer was used in this study. PIV analysis was employed as a non-intrusive method to capture the particle soil displacement fields and display the deformation behavior while footing loading. It was found that both the bearing capacity and the failure mode are extremely sensitive to the footing's position proportional to the setback distance ratios (*D*/*B*). The footings nearby the slope exhibited unsymmetrical failure wedges with slip surfaces extending to the slope face, resulting in a face failure mode, while the footings with larger setback distances transitioned to bearing capacity failures. The inclusion of a geotextile reinforcement layer improved the bearing performance, particularly at setback distance ratios of *D*/*B* = 1 and *D*/*B* = 2. The optimum improvement was observed when reinforcement was placed at a depth not exceeding half the footing width. Two distinct modes of the footing on a slope are revealed: peak load resistance and a sudden jerking phenomenon, with the latter consistently associated with slope influence. Overall, the application of PIV provided a deeper insight into the soil–structure interaction and proved to be a reliable tool for assessing the deformation mechanisms in slope-footing systems.

Keywords-Particle Image Velocimeter (PIV); strip foundation; laboratory model; slope; sand soil

I. INTRODUCTION

The use of geosynthetics, especially geotextiles, as reinforcement materials has increased significantly in geotechnical engineering applications [1]. Among these, the slope stabilization and the enhancement of the bearing capacity for footings located near slopes have gained large attention [2, 3]. The inclusion of geotextile inside the soil layers has been proven effective in improving the slope performance and reducing the deformations, leading to a wide range of experimental and analytical studies focused on their application in footing-slope interaction problems [4].

Previous comprehensive experimental investigations have been implemented to study the behavior of the bearing capacity and failure mechanisms of shallow foundations on sand slopes exposed to vertical or eccentric loads. However, the PIV analysis on reinforced sand slopes subjected to vertically loaded strip footings is limited [5, 6]. The bearing capacity of a strip footing placed on a slope essentially comes from the weight of soil above the footing base and the shear forces generated along the length of the slip surface [7]. Several small-scale physical model laboratory test results conducted on different embedment depths of footing on a sand slope are reported [8].

The small physical models provide substantial advantages due to the complete control over all model tests, such as choosing specific soils, loading conditions, and defining boundaries [9]. These controlled conditions ensure well-defined theoretical problems and efficient, cost-effective testing with shorter durations and smaller quantities of soil [10]. This efficiency allows for numerous tests, enabling a thorough investigation of various parameters and enhancing the

reliability of the research findings [12]. It has been found that the average ultimate bearing capacity of the footing on the slope reaches a constant value after a certain setback distance of about 5 times the width of the footing, and it is largely dependent on the relative density of the sand [4]. On the basis of the test results and their comparison with study in [11] theoretical analysis, authors in [13] concluded that the theoretical predictions produce significant differences with the laboratory results. Moreover, the experimental exploration of the bearing capacity and settlement execution of foundations on slopes is significant. Most studies have been performed using loose to dense sand of relative density [14-17].

An effective ground improvement method is the employment of geosynthetic materials, due to their easy adjustability, cost-effectiveness, and reliability. The utilization of geosynthetics into weaken sand as a reinforcement material generates protection from the landslides, failure, liquefaction, and several engineering problems. The use of geotextiles as one of the main construction materials for lining ground has been proven effective [17].

The present study focuses on evaluating the results from a series of small-scale physical models for strip footing resting on reinforced and unreinforced sand slopes. The effectiveness of the geotextile reinforcement in enhancing the bearing capacity of a strip footing placed near the crest of a sand slope [12], with different setback distance ratios *D*/*B* for dense sand throughout the full applied loading, was assessed in terms of the soil displacement measured using PIV. Particular attention was given to identifying the optimum location of the geotextile layer that results in the maximum improvement. The results were analyzed using both the load–settlement behavior and PIV to visualize the associated failure mechanisms.

II. LABORATORY MODEL TESTS

A. Materials Used for the Testing

The sand utilized in this study was manually washed and air-dried. To obtain reliable results, the physical models were carefully prepared. The characteristics of the sand model were determined according to ASTM standards. The laboratory tests on the sand concluded that the latter has the following physical properties: effective particle size (*D10*) of 0.15 mm, specific gravity of G_s = 2.65, angle of internal friction of 30°, and unit weight of 18.35 kg/m³. The coefficient of curvature is C_c = 0.96, and the uniformity coefficient is C_u = 2.97, with relative densities of 79%, and it is classified as poorly graded sand (SP) by using the Unified Soil Classification System (USCS).

The woven geotextiles and nonwoven geotextiles are widely used by engineers as reinforcement materials to improve the features of sandy soil. These materials can easily stabilize the soil and provide high strength. Also, they can provide protection against the permeability phenomenon [1]. The basic properties obtained from the manufacturer's datasheet for the geotextile are: white sheet polyethylene polymer nonwoven geotextile, 50 g/m², 0.82 mm thickness, 7.6 kN/m ultimate tensile strength, and 58% failure strain.

B. Test Setup

The experimental slope footing system is represented by a device especially manufactured for this purpose with a rectangular test container of 462 mm width, 1200 mm length, and 460 mm height. The base and three sides of the container were made of 5 mm thick steel plate, and the front window of the container was made of 10 mm thick transparent glass, serving as a visual window for photography and allowing the monitoring and tracking of particle movement during imaging. The strip footing model was made from a 30 mm-thick steel plate with a width of 70 mm and a length equal to that of the container. The steel container and the footing model were adequately rigid to provide plane strain states for the whole model. A manual hydraulic jacking system was designed to apply a vertical load on the strip footing model at any point on the slope crest. Digital photography with a Sony a7 iii camera (full frame, 24 megapixel) facilitated the visualization of the soil movement during tests. Target markers were used as a control point for camera calibration. A photography and schematic view of the test equipment is shown in Figure 1.

(a)

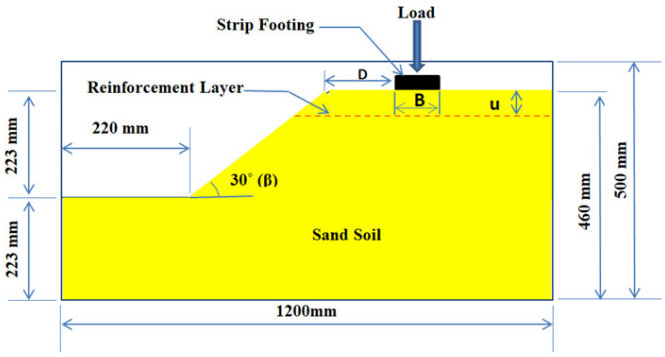

(b)

Fig. 1. (a) Photograph of the test equipment, (b) schematic view of the test setup.

C. Composition of Sand Slope

Sand slope models 460 mm high, 462 mm wide, and 1200 mm long, with a constant slope angle β of 30 were prepared

using tamping packing methods. The internal face of the test container was divided into four layers of 115 mm thickness. The model slope was formed in two stages: (1) first two sand layers were constructed up to the slope toe, and (2) second two layers with the slope face were constructed by an adaptable setup to get the required slope dimension for each test in this study. In the case of reinforcement layers, the heights of the last two layers were adjusted to match the reinforcement layer depth ratio (U/B) at which the reinforcement was placed, and set at 0.5 and 1. A single reinforced layer was used in this study. The load was applied manually by hydraulic jack until failure. The stress control was maintained manually by rate adjustments, using trial-and-error attempts to achieve an approximate loading rate of 1 mm/min.

D. Test Program

In this study two main groups of model tests were conducted under different test programs. First, the response of a strip foundation constructed on an unreinforced sand slope was investigated. Second, a strip foundation constructed on a reinforced sand slope was carried out to study the difference in the behavior of the two cases, focusing on its influence on the slope stability and failure mechanisms. Each series was conducted to study the response of a strip footing under vertical loading with other variables held constant. The constant parameters are the relative density (Dr), foundation width (B), and slope angle (β), while the variable parameters include the foundation setback distance ratio (D/B) and reinforcement layer depth ratio (U/B). Table I provides a summary of all the test programs conducted for the slopes, with the constant and the variable parameters utilized. After each instance of loading, the load and settlement were recorded by the data logger, the system was photographed with a digital camera, and the images were processed using Geopiv8 software.

TABLE I. DESCRIPTION OF LABORATORY MODEL TEST SERIES

Groups	Test series	Invariable parameters	Variable parameters
Group A	1	Dr = 79%, β =30°, B = 70 mm	D/B = 0, 1, 2, 3, 4, 5
Without reinforcement	2	Dr = 79%, β =30°, B = 70 mm	U= 0.5B, D/B = 0, 1, 2, 3, 4, 5
	3	Dr = 79%, β =30°, B = 70 mm	U = 1.0B, D/B = 0, 1, 2, 3, 4, 5

III. RESULTS AND DISCUSSION

A. Bearing Capacity Improvement Factor (IF)

An extensive series of 15 small-scale model tests were conducted on the model plane strain strip footing, resting on reinforced and unreinforced sand slopes to analyze its bearing capacity performance and failure mechanisms. The bearing capacity performance was assessed using a non-dimensional factor called the IF, determined by the ratio of the ultimate bearing capacity for the geotextile-reinforced slope to that without the reinforced slope. It quantifies the increase in the footing bearing capacity resulting from reinforcement placement, and is defined as:

$$IF = \frac{q_r}{q_{ur}} \quad (1)$$

where q_r is the bearing capacity of the footing on the reinforced slope, and q_{ur} is the bearing capacity of the footing on the unreinforced slope. The allowable settlement method was used for the calculation of the bearing capacity. Pressure corresponding to a settlement equal to 10% of the footing width (0.1B), in accordance with standard practice, was used to define the footing's ultimate bearing capacity. This methodology is employed to calculate the IF due to the slope reinforcement and is consistent with that proposed in [18].

Figures 2 and 4 depict the bearing capacities from the load–settlement curves up to 15% of the strip footing width. A settlement of 10% of the footing width is taken as the allowable failure condition beyond which the footing is considered to have collapsed. Figure 2 presents the variation of the bearing pressure with footing settlement for the test group A, where the slope was tested without reinforcement and with a setback distance D/B from 0 to 5 for the dense states. Figure 3 displays the variation of the bearing pressure with footing settlement for the test group B, where the slope was tested with a single reinforcement geotextile layer and a setback distance D/B from 0 to 5. The depth of the reinforcement geotextile layer was 0.5B. As shown in Figure 2, as the relative density of the sand increases, the bearing capacity increases.

The load-settlement curve observations confirm that the periods of collapse and stability converge with the load reductions and increases. This is due to the effects of the slope, which generated the observed load-displacement oscillation. According to [19], the failure modes in soils for the shallow foundations are: general shear for dense sand, local shear for medium sand, and punching shear for loose sand. The sand slopes exhibited local shear failure with "sudden jerks." The sudden failure could be caused by the potential energy stored in the soil mass from the progressively applied load, without notable settlement, until it reached a limit equilibrium state; then the energy was transformed to kinetic energy, resulting in a visible settlement of the footing. The load–settlement curve behavior for the footing on a slope reveals two distinct modes: the peak load resistance and a sudden jerking phenomenon. The peak load resistance is not clearly noticed in the case of a setback distance D/B more than 5, whereas it becomes noticeable for a setback distance D/B less than 3. The occurrence of sudden jerks is inherent in all cases and, in these instances, it is attributed to the influence of the slope.

The loading tests were conducted on a slope with a single reinforcement geotextile layer to investigate the effect of reinforcement. The reinforcement layers were placed at a depth of 0.5B. All tests in this case were conducted for a slope angle of 30° and D/B = 1-5. The load settlement curve results are portrayed in Figure 3.

Table II demonstrates the improvement in the bearing capacity in terms of the IF for reinforced geotextile slopes.

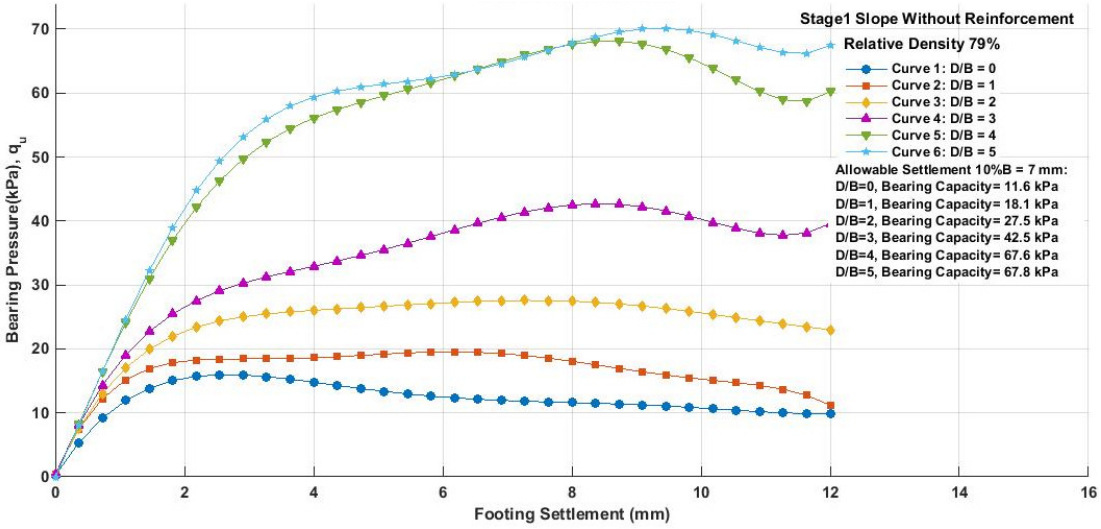

Fig. 2. Load-settlement curves of unreinforced slope test with varied setback distance *D*/*B* from 0 to 5.

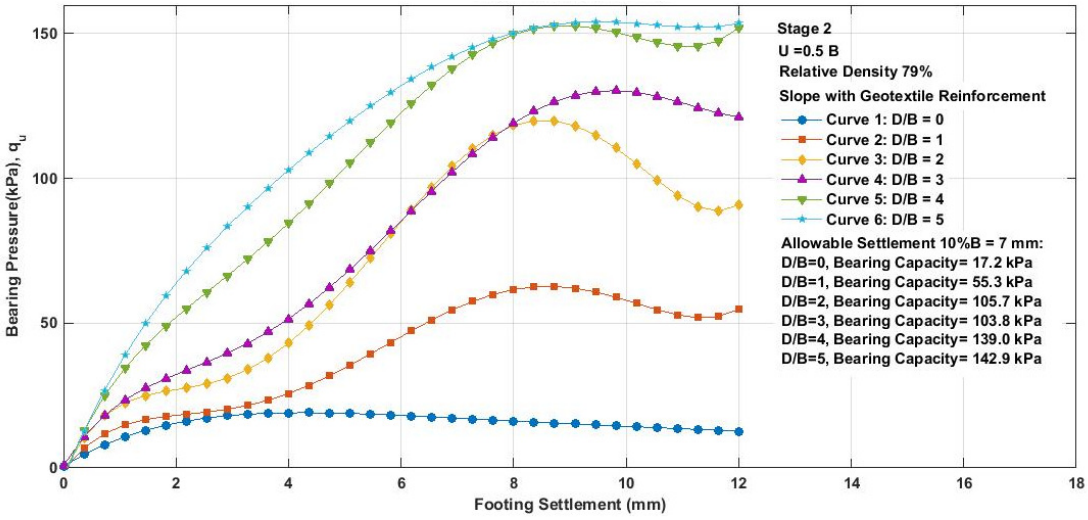

(a)

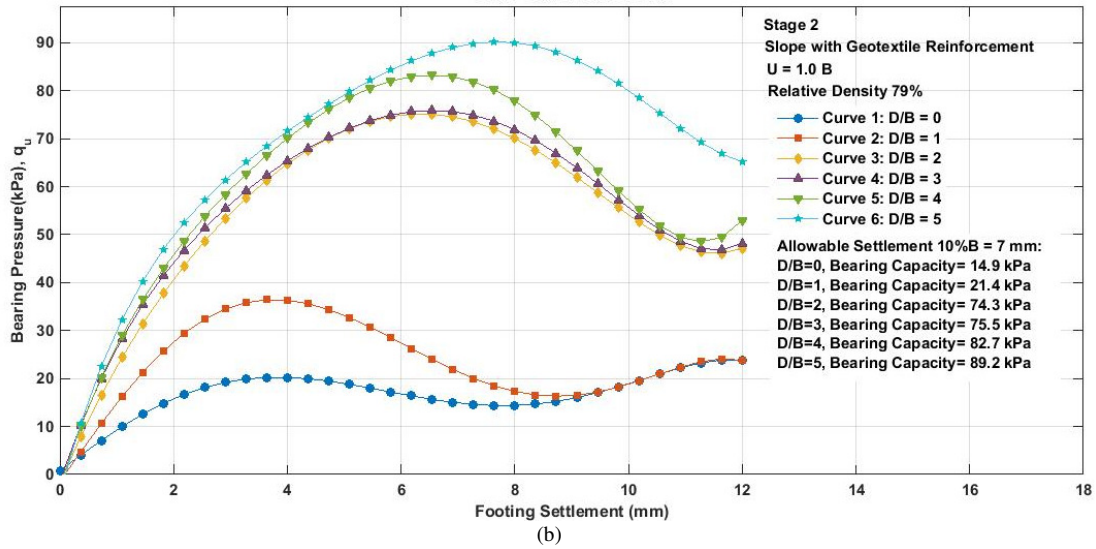

(b)

Fig. 3. Load-settlement curves of reinforced slope test with: (a) depth of reinforcement layer (*U*/*B*) ratio of 0.5, (b) depth of reinforcement layer (*U*/*B*) ratio of 1.0.

TABLE II. IMPROVEMENT OF THE BEARING CAPACITY

Relative density *Dr* (%)	**Depth of reinforcement layer *U* (% *B*)**	**Setback distance *D/B* (%)**	**Ultimate bearing capacity (kPa)**		**IF factor (%)**
			Reinforced slope	Unreinforced slope	
79	0.5	1	55.3	18.1	3.0
		2	105.7	27.5	3.8
		4	139.0	67.6	2.0
	1.0	1	21.4	18.1	1.1
		2	74.3	27.5	2.7
		4	82.7	67.6	1.2

Table II reveals an inverse relationship between the IF and the setback distance. The factor IF suffers from a decrease beyond the critical setback distance ratio of *D*/*B* = 2. Furthermore, the increase rate in the IF value due to geotextile reinforcement is more pronounced when the footing is located near the slope. This increase achieves its peak at a setback distance ratio of *D*/*B* = 2 beyond which the improvement rate begins to decay.

B. Edge Distance Effect

Figure 2 presents the unreinforced ultimate bearing capacity, which increases with a setback distance increase from 11.6 kPa to 67.8 kPa for *D*/*B* = 0-5, with an increase ratio of 5.8% for the dense state. Also, for the critical setback distance *D*/*B* = 2, the increase ratio is 1.35%. It is worth noting that the increase in the setback distance results in a rise in the ultimate bearing capacity value of the critical setback distance *D*/*B* = 2, greater than that of a critical setback distance *D*/*B* more than 2. Similarly, regarding the reinforcement case, the ultimate bearing capacity increases with a setback distance increase from 17.2 kPa to 142.9 kPa with an increase ratio of 8.4% for the *U*/*B* ratio of 0.5. The reinforcement case of depth of reinforcement layer *U*/*B* ratio of 1.0 shows a smaller increase in the ultimate bearing capacity from 14.9 kPa to 89.2 kPa, with an increase ratio of 5.9%.

C. Effect of Reinforcement Position

The bearing capacity and the optimum position for the geotextile reinforcement occur at a depth *U*/*B* ratio of 0.5. The location of the geotextile layer at a depth equal to the width of the footing leads to an improvement in the load-bearing capacity of the footing on a slope less than for a *U*/*B* ratio of 0.5. The observations made during the investigation of geotextile reinforced slopes proved that the optimum reinforcement depth *U*/*B* is 0.5 with a relative density equal to 79%, which gives an IF of 3.8% for the bearing capacity, and decreases with an increase in *U*/*B*. In general, the sand slope reinforced with a single geotextile layer at depths of 0.5 or 1.0 of the footing width performed better than the unreinforced slope case. Furthermore, the load settlement curves mentioned in [7] showed comparable findings.

D. PIV Results

The PIV analysis method was utilized to assess the deformation of the soil using a series of digital images. The digital images were recorded at a rate of 1 fps during the loading process to an allowable settlement of 10% from the width of the footing, which produced a series of about 420 images from each loading test. These images were used by PIV to derive the displacement and shear strain fields. Figure 4 illustrates the displacement field derived from the PIV analyses. It is clear that the decrease in the setback distance made the displacement of the soil to tend towards the face of the slope. The vertical displacements caused by the loaded footing on the unreinforced slope crest are illustrated in Figure 5. Due to the decrease in the setback distance, the general trend is that a considerable downward displacement is apparent through the length of the failure slip propagating toward the slope face. The deformation mechanism observed is a curved line that occurs directly beneath the footing, resulting in an asymmetrical failure wedge. The failure wedge begins at a point beneath the footing corner that is away from the slope and curves outward toward the slope face.

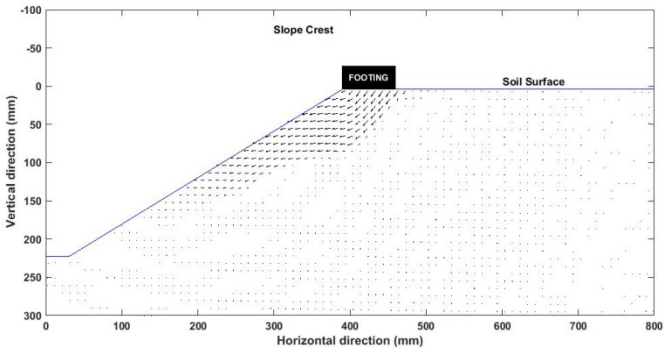

Fig. 4. Displacement vector from PIV results for footing on unreinforced slope test of 10% settlement and setback distance *D*/*B* = 0.

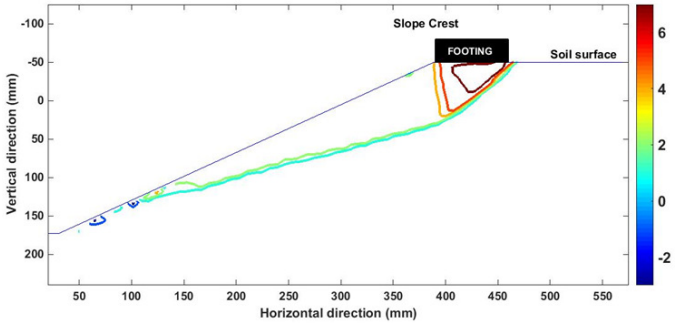

Fig. 5. Vertical displacement contours from PIV results for footing on unreinforced slope test of 10% settlement and setback distance *D*/*B* = 0.

Figure 6 shows the vertical displacement contours of the footing on the reinforced slope with 10% settlement for a setback distance *D*/*B* of 0, 2, and 4. When the footing is close to the slope face, the placement of geotextile reinforcements

improves the footing bearing capacity and reduces the deformation of the soil. The placement of a geotextile reinforcement layer changed the deformation pattern and reduced the size of the failure zone from a slope failure to a bearing capacity failure mechanism. This change in the behavior is observed in the reinforced soil cases with a setback distance ratio less than 2. Also, a small heave is evidenced within 1.5*B* distance on both footing sides, when the footing setback distance increases. This observation is consistent with the findings of [20].

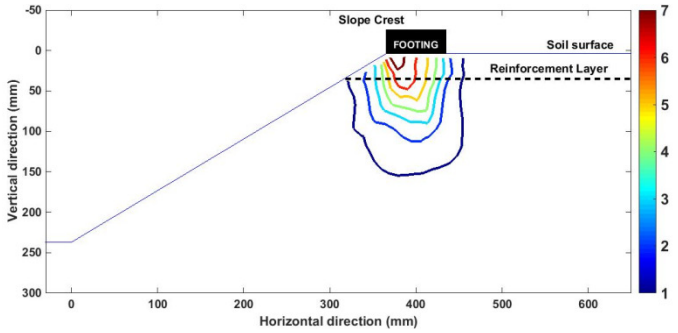

Fig. 6. Vertical displacement contours from PIVresults for footing on geotextile reinforced slope test U/B = 0.5 of 10% settlement and setback distance D/B = 0.

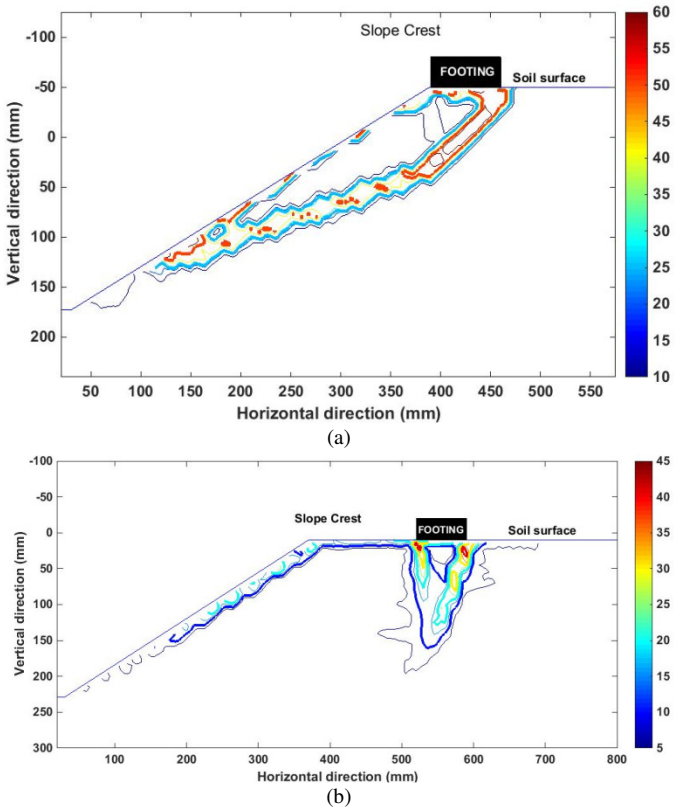

Fig. 7. Maximum shear strain contours from PIV results for footing on unreinforced slope test U/B = 0.5 of 10% settlement, (a) setback distance D/B = 0, and (b) setback distance D/B = 2.

Figures 7 and 8 present the maximum shear strain fields for the unreinforced and reinforced cases, respectively. For the unreinforced slope, the zone of influence extends to a depth of up to 3*B* below the footing for a setback distance D/B more than 2.

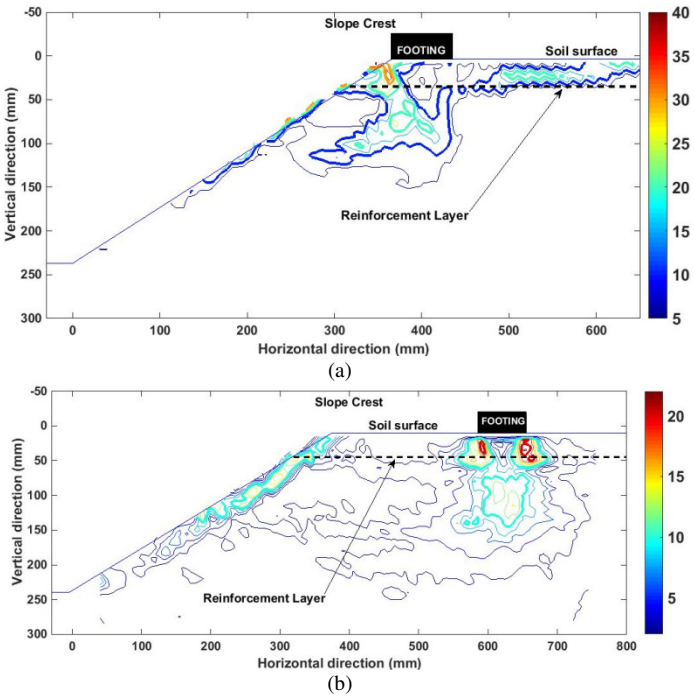

Fig. 8. Maximum shear strains contours from PIV results for footing on geotextile reinforced slope test U/B = 0.5 of 10% settlement, (a) setback distance D/B = 0, and (b) setback distance D/B = 4.

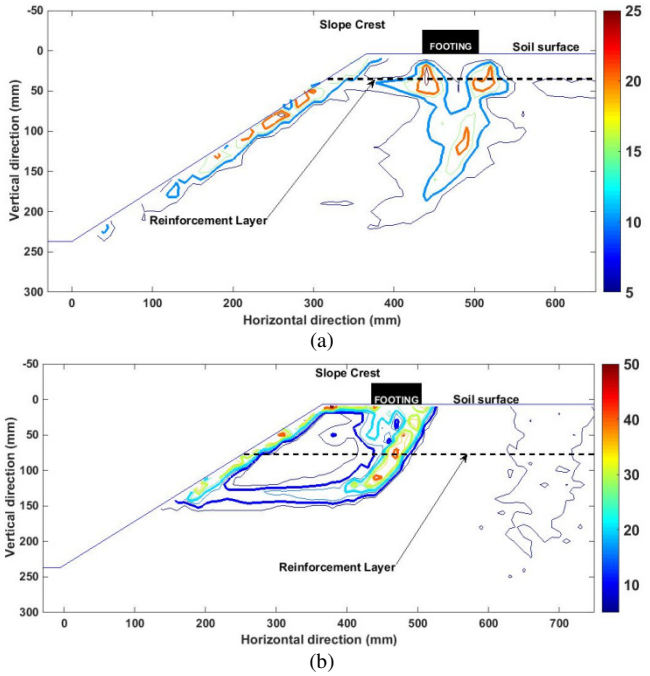

Fig. 9. Figure 9. Maximum shear strains contours from PIV results for footing on geotextile reinforced slope test of 10% settlement, (a) embedment ratio U/B = 0.5, and (b) embedment ratio U/B = 1.0.

The largest concentration of shearing force is at the setback distance $D/B = 0$, with the slip surface extending to the slope face, resulting in a face failure. On the contrary, for the reinforced slopes, the zone of influence extends to a depth of less than $2B$ below the soil surface for setback distances $D/B =$ 2 and 5. In contrast to the unreinforced slope, the setback distance $D/B = 0$ does not show any slip surface, and the failure zone changes to a bearing capacity failure mechanism similar to that with setback distances further than 2. The deformation mechanism observed is similar to that proposed in [8]. The shear strain forces for the footing on geotextile reinforced sand slope are presented in Figures 9 (a) and (b). It can be observed that the embedment ratio U/B of the reinforced geotextile layer increased from 0.5 to 1.0, the maximum shear strains increased, and the slip failure propagated toward the slope face.

E. Comparison with Previous Studies

The deformation mechanisms observed in the present investigation, as illustrated in Figures 5 and 6, show that the placement of geotextile reinforcement significantly changes the failure mode from a slope failure type to a bearing capacity failure. This behavior is particularly evident when the footing is positioned near the slope edge ($D/B \leq 2$), where the reinforced layer helps confine the shear zone and reduces its distribution toward the slope face. These observations are in good agreement with the experimental results reported in [8], where it was demonstrated that geogrid reinforcement near the slope surface not only increases the bearing capacity, but also restrains the development of shear failure planes within the slope, leading to a conversion from the slope stability to the bearing failure of the footing. Also, these observations confirm that an embedment ratio U/B deeper than 0.5 for the reinforcement layer gives the opportunity to form the failure slip line above the reinforcement layer level.

Furthermore, the observed change in the failure mode with setback distance replicates the failure discussed in [7], where six different collapse mechanisms for strip footings near slopes were classified. In these simulations, regarding the footings located very close to the slope crest, the face failure mode was dominant, a finding that is consistent with the B1 modes (face failures) identified in [7]. The study highlighted the influence of the slope geometry and soil properties on the failure mode, a form that is replicated in the unreinforced cases, as shown in Figure 7 (a).

IV. CONCLUSIONS

The experimental investigation performed in this study provided significant insights into the behavior of the strip footings located on the crest of reinforced and unreinforced sand slopes using Particle Image Velocimetry (PIV) techniques. The deformation mechanisms for the strip footing vertically loading on loose and dense sand were investigated through image analysis. Both the ultimate bearing capacity and the failure mechanism of the footing location on the top of the slope crest are significantly influenced by the setback distance, relative density, and depth of the reinforced layer. The rate of increase in the Improvement Factor (IF) due to geotextile reinforcement is more pronounced when the footing is located near the slope. The footings situated closer to the unreinforced slopes exhibited an unsymmetrical failure mechanism with slip failure directed toward the slope, resulting in a face failure mode. Both, the unreinforced and reinforced footing-slope systems encountered a significant rise in the bearing capacity as the setback distance ratio (D/B) increased. This phenomenon is attributed to the larger zone of passive resistance within the soil mass underneath the footing as it transfers away from the slope face. However, the presence of the slope still has an effect on footings beyond $D/B = 5$ in relation to the settlement value in the range of D/B considered in the current study.

The placement of geotextile reinforcement changes the deformation mechanism to a bearing capacity failure mechanism rather than a slope failure, particularly at setback D/B of 1 and 2, close to the behavior that occurs on leveled ground. Based on the observed failure mechanism, this study proposes positioning the geotextile reinforcement to intersect the potential failure surface near the footing toe, within a depth not exceeding half the footing width. The behavior of the load settlement curve of the footing on a slope reveals two distinct modes: a peak load resistance and a sudden jerk phenomenon. The peak load resistance is not clearly noticed in the case of loose sand, whereas it becomes more noticeable in the dense sand. The occurrence of sudden jerks is inherent in all cases and, in this case, is attributed to the influence of the slope. Finally, the study demonstrated that the utilization of PIV techniques offers reliable insights into the failure mechanism, in contrast to other methods, enabling investigators to predict the behavior of the footing–slope system in sandy soil.

REFERENCES

[1] M. Alali, B. Paikaray, and B. Mohapatra, "An insight on the response of foundations resting on sand with geosynthetic materials as a reinforcement," *Journal of Physics: Conference Series*, vol. 1973, no. 1, Aug. 2021, Art. no. 012153, https://doi.org/10.1088/1742-6596/1973/1/012153.

[2] A. Dey, R. Acharyya, and A. Alammyan, "Bearing capacity and failure mechanism of shallow footings on unreinforced slopes: a state-of-the-art review," International Journal of Geotechnical Engineering, vol. 15, no. 10, pp. 1284–1297, Nov. 2021, https://doi.org/10.1080/19386362.2019.1617480.

[3] B. S. Albusoda and S. Z. Al-Saady, "Numerical Modeling of Square Footing Subjected to Eccentric Loading on Geogrid Reinforced Loose Sand," *Key Engineering Materials*, vol. 857, pp. 341–348, Aug. 2020, https://doi.org/10.4028/www.scientific.net/KEM.857.341.

[4] M. Salih Keskin and M. Laman, "Model studies of bearing capacity of strip footing on sand slope," *KSCE Journal of Civil Engineering*, vol. 17, no. 4, pp. 699–711, May 2013, https://doi.org/10.1007/s12205-013-0406-x.

[5] D. J. White, W. A. Take, and M. D. Bolton, "Soil deformation measurement using particle image velocimetry (PIV) and photogrammetry," *Géotechnique*, vol. 53, no. 7, pp. 619–631, Sept. 2003, https://doi.org/10.1680/geot.2003.53.7.619.

[6] M. A. El Sawwaf, "Behavior of strip footing on geogrid-reinforced sand over a soft clay slope," *Geotextiles and Geomembranes*, vol. 25, no. 1, pp. 50–60, Feb. 2007, https://doi.org/10.1016/j.geotexmem.2006.06.001.

[7] H. Zhou, G. Zheng, X. Yin, R. Jia, and X. Yang, "The bearing capacity and failure mechanism of a vertically loaded strip footing placed on the top of slopes," *Computers and Geotechnics*, vol. 94, pp. 12–21, Feb. 2018, https://doi.org/10.1016/j.compgeo.2017.08.009.

[8] C. Yoo, "Laboratory investigation of bearing capacity behavior of strip footing on geogrid-reinforced sand slope," *Geotextiles and Geomembranes*, vol. 19, no. 5, pp. 279–298, July 2001, https://doi.org/10.1016/S0266-1144(01)00009-7.

[9] D. M. Wood, *Geotechnical Modelling*. Abingdon, UK: Taylor & Francis, 2004.

[10] M. Mirzababaei, M. Mohamed, and M. Miraftab, "Analysis of Strip Footings on Fiber-Reinforced Slopes with the Aid of Particle Image Velocimetry," *Journal of Materials in Civil Engineering*, vol. 29, no. 4, Apr. 2017, Art. no. 04016243, https://doi.org/10.1061/(ASCE)MT.1943-5533.0001758.

[11] B. Mazouz, T. Mansouri, M. Baazouzi, and K. Abbeche, "Assessing the Effect of Underground Void on Strip Footing Sitting on a Reinforced Sand Slope with Numerical Modeling," *Engineering, Technology & Applied Science Research*, vol. 12, no. 4, pp. 9005–9011, Aug. 2022, https://doi.org/10.48084/etasr.5131.

[12] G. G. Meyerhof, "The Ultimate Bearing Capacity of Foundations on Slopes," *4th International Conference on Soil Mechanics and Foundation Engineering (London)*, 1957.

[13] J. D. Scott, J. H. Deschenes, A. K. Barsvary, D. H. Shields, and G. E. A. Bauer, "Bearing Capacity of Foundations Near Slopes," *9th International Conference on Soil Mechanics and Foundation Engineering*, Tokyo, Japan, 1977.

[14] B. A. Ahmed and D. A. R. Al-Hamdani, "Investigation of the Deformation of Sandy Soil Near a Laterally Loaded Single Pile Using the Particle Image Velocimetry Technique," in *Current Trends in Geotechnical Engineering and Construction*, M. Karkush, D. Choudhury, and J. Han, Eds. Singapore: Springer Nature Singapore, 2023, pp. 178–194.

[15] S. Ghani and S. Kumari, "Liquefaction study of fine-grained soil using computational model," *Innovative Infrastructure Solutions*, vol. 6, no. 2, June 2021, Art. no. 58, https://doi.org/10.1007/s41062-020-00426-4.

[16] G. M. Latha and A. Somwanshi, "Bearing capacity of square footings on geosynthetic reinforced sand," *Geotextiles and Geomembranes*, vol. 27, no. 4, pp. 281–294, Aug. 2009, https://doi.org/10.1016/j.geotexmem.2009.02.001.

[17] K. M. Lee and V. R. Manjunath, "Experimental and numerical studies of geosynthetic-reinforced sand slopes loaded with a footing," *Canadian Geotechnical Journal*, vol. 37, no. 4, pp. 828–842, Aug. 2000, https://doi.org/10.1139/t00-016.

[18] S. Alamshahi and N. Hataf, "Bearing capacity of strip footings on sand slopes reinforced with geogrid and grid-anchor," *Geotextiles and Geomembranes*, vol. 27, no. 3, pp. 217–226, June 2009, https://doi.org/10.1016/j.geotexmem.2008.11.011.

[19] J. C. Das, *Transients in electrical systems: analysis, recognition, and mitigation*. New York: McGraw-Hill, 2010.

[20] H. Khalvati Fahliani, M. R. Arvin, N. Hataf, and A. Khademhosseini, "Experimental Model Studies on Strip Footings Resting on Geocell-Reinforced Sand Slopes," *International Journal of Geosynthetics and Ground Engineering*, vol. 7, no. 2, June 2021, Art. no. 24, https://doi.org/10.1007/s40891-021-00270-1.